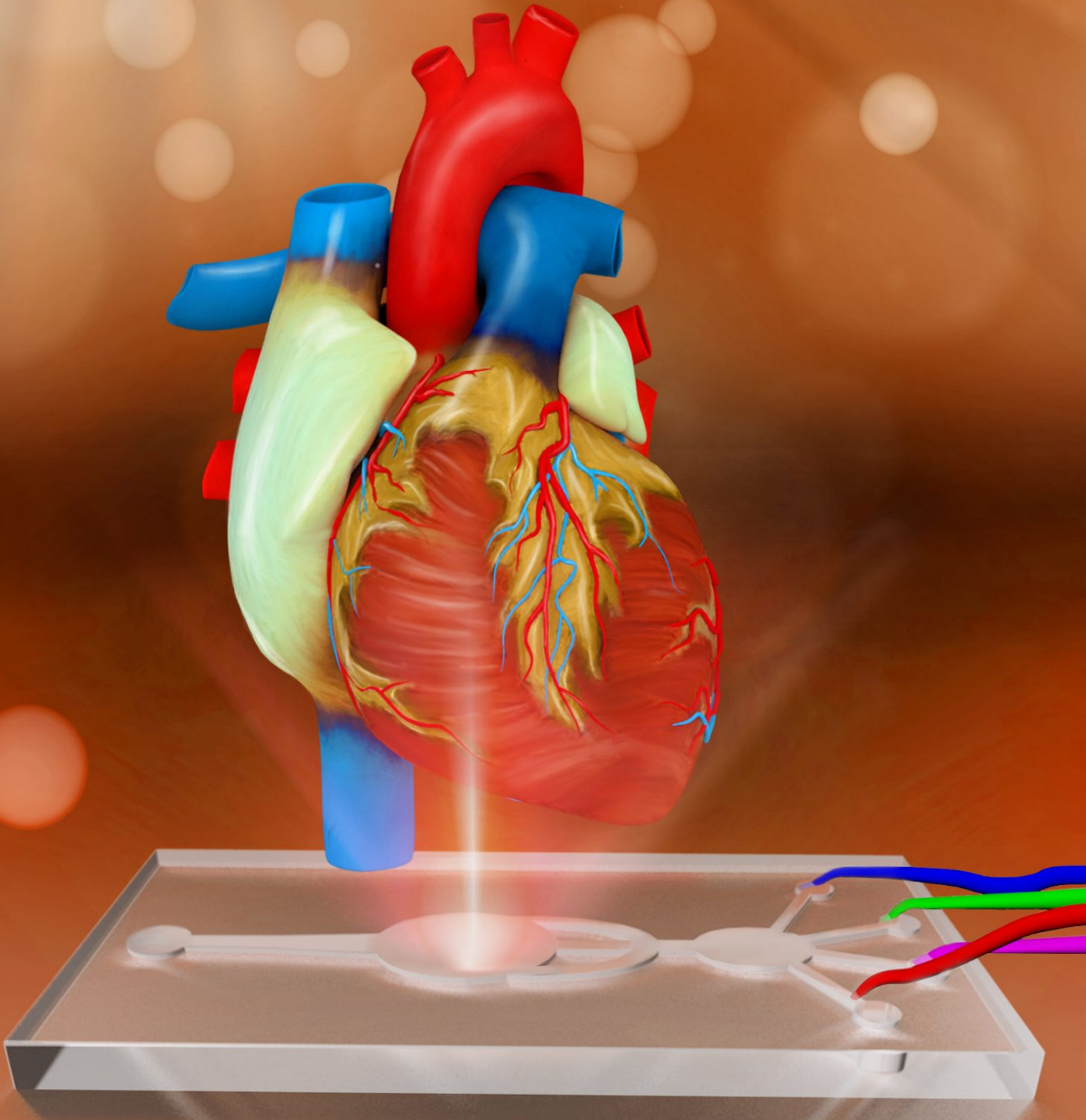# Microfluidics-Enabled Multimaterial Maskless Stereolithographic Bioprinting

Amir K. Miri, Daniel Nieto, Luis Iglesias, Hossein Goodarzi Hosseinabadi, Sushila Maharjan, Guillermo U. Ruiz-Esparza, Parastoo Khoshakhlagh, Amir Manbachi, Mehmet Remzi Dokmeci, Shaochen Chen, Su Ryon Shin, Yu Shrike Zhang,* and Ali Khademhosseini*

A stereolithography-based bioprinting platform for multimaterial fabrication of heterogeneous hydrogel constructs is presented. Dynamic patterning by a digital micromirror device, synchronized by a moving stage and a microfluidic device containing four on/off pneumatic valves, is used to create 3D constructs. The novel microfluidic device is capable of fast switching between different (cell-loaded) hydrogel bioinks, to achieve layer-by-layer multimaterial bioprinting. Compared to conventional stereolithography-based bioprinters, the system provides the unique advantage of multimaterial fabrication capability at high spatial resolution. To demonstrate the multimaterial capacity of this system, a variety of hydrogel constructs are generated, including those based on poly(ethylene glycol) diacrylate (PEGDA) and gelatin methacryloyl (GelMA). The biocompatibility of this system is validated by introducing cell-laden GelMA into the microfluidic device and fabricating cellularized constructs. A pattern of a PEGDA frame and three different concentrations of GelMA, loaded with vascular endothelial growth factor, are further assessed for its neovascularization potential in a rat model. The proposed system provides a robust platform for bioprinting of high-fidelity multimaterial microstructures on demand for applications in tissue engineering, regenerative medicine, and biosensing, which are otherwise not readily achievable at high speed with conventional stereolithographic biofabrication platforms.

Dr. A. K. Miri, Prof. D. Nieto, L. Iglesias, H. Goodarzi Hosseinabadi,
Dr. S. Maharjan, Dr. G. U. Ruiz-Esparza, Dr. P. Khoshaghlagh,
Dr. A. Manbachi, Dr. M. R. Dokmeci, Dr. S. R. Shin,
Dr. Y. S. Zhang, Prof. A. Khademhosseini
Division of Engineering in Medicine
Department of Medicine
Brigham and Women's Hospital
Harvard Medical School
Cambridge, MA 02139, USA
E-mail: yszhang@research.bwh.harvard.edu; khademh@ucla.edu
Dr. A. K. Miri, Prof. D. Nieto, L. Iglesias, H. Goodarzi Hosseinabadi,
Dr. S. Maharjan, Dr. G. U. Ruiz-Esparza, Dr. P. Khoshaghlagh,
Dr. A. Manbachi, Dr. M. R. Dokmeci, Dr. S. R. Shin, Dr. Y. S. Zhang,
Prof. A. Khademhosseini
Harvard-MIT Division of Health Sciences and Technology
Massachusetts Institute of Technology
Cambridge, MA 02139, USA

Prof. D. Nieto
Microoptics and GRIN Optics Group
Applied Physics Department
Faculty of Physics
University of Santiago de Compostela
Santiago de Compostela 15782, Spain

H. Goodarzi Hosseinabadi
Polymeric Materials Research Group
Department of Materials Science and Engineering
Sharif University of Technology
Tehran 1458889694, Iran

Dr. A. Manbachi
Department of Biomedical Engineering
Whiting School of Engineering
Johns Hopkins University
Baltimore, MD 21218, USA

Prof. S. Chen
Department of NanoEngineering
University of California
San Diego, La Jolla, CA 92093, USA

Prof. S. Chen
Department of Bioengineering
University of California
San Diego, La Jolla, CA 92093, USA

Prof. S. Chen
Materials Science and Engineering Program
University of California
San Diego, La Jolla, CA 92093, USA

Prof. A. Khademhosseini
Center for Minimally Invasive Therapeutics (C-MIT)
University of California-Los Angeles
Los Angeles, CA 90095, USA

Prof. A. Khademhosseini
Department of Radiology
David Geffen School of Medicine
University of California-Los Angeles
Los Angeles, CA 90095, USA

Prof. A. Khademhosseini
Department of Bioengineering
Department of Chemical and Biomolecular Engineering
Henry Samueli School of Engineering and Applied Sciences
University of California-Los Angeles
Los Angeles, CA 90095, USA

In nature, multiscale structures with hierarchical features are consequences of conditions reached during material optimization when organizing underlying components with regards to external environments.[1] Such material optimization can be found in the bifurcation of human organs such as liver,[2] retina,[3] vein,[1] and arteries.[4] To fabricate biomimetic structures resembling their natural counterparts, existing manufacturing methods such as freeze-drying[5] and salt-leaching[6] lack flexibility to tune the design regionally. Photolithography[7] and laser sintering[8] have been further introduced to fabricate geometries at high precisions. However, laser sintering techniques suffer from practical limitations in terms of the manufacturing speed and the material composition. Regarding the success of photolithography, common light-assisted three-dimensional (3D) printing systems including continuous digital light processing (DLP),[9] DLP-based 3D printing,[10] mask-projection micro-stereolithography[11], and dynamic mask stereolithography[12] have been used so far. Most of these systems represent top-down projection approaches, while bottom-up projection approaches can provide quicker build-up time, higher resolution, and material conservation.[13]

The digital micromirror device (DMD)-based projection printing has emerged as a high-throughput DLP technique offering great biocompatibility for cell seeding and encapsulation.[14] DMD is a micro-electro-mechanical system that enables a user to control over one million small mirrors to turn-on or turn-off on the order of kilohertz (kHz). An ultraviolet (UV) lamp projects high-intensity light on the DMD panel, which patterns the image of each layer of the computer-aided-design (CAD) model, and projects onto the bottom side of the container. Following this UV exposure, the photosensitive polymer or hydrogel crosslinks and attaches to the previous layer. DMD-based printing offers high-quality surface finishing and a variety of material options.[11] Conventional DLP-based techniques are slow and their use in fabricating cell-laden constructs with clinically relevant dimensions is thus very challenging.[7] Following benchmark multimaterial stereolithography designs by adapting commercial printers to function with several ink reservoirs,[15] Bashir and co-workers designed a DMD-based bioprinting apparatus to generate multicomponent biohybrid myocardium-based actuators, by manually changing the bath solutions.[16] We have previously developed a high-precision DMD-based bioprinter for multipurpose uses, and fabricated a 3D hydrogel-based triculture model using hepatic progenitor cells, human umbilical vein endothelial cells, and adipose-derived stem cells in a microscale hexagonal architecture.[2] The potential of DMD-based bioprinters in fabrication of microfluidic platforms used in medical diagnostics was also demonstrated.[17] Despite these significant advantages, several key challenges for fabricating biomimetic tissue constructs

still remain, including the inability for continuous fabrication of cell-laden constructs with clinically relevant dimensions and the inability to bioprint multicomponent complex constructs with high precision. A core challenge in the use of multiple materials is how to manage material contamination between changing different materials used in the printing process. Among various photopolymers, gelatin methacryloyl (GelMA)[2] and poly(ethylene glycol) diacrylate (PEGDA)[18] have shown great biocompatibility for cell encapsulation.

Here we demonstrate that the integration of a simple microfluidic platform can advance the DMD-based bioprinter for proper fabrication of inhomogeneous GelMA and PEGDA constructs at high fidelity. Models could be conveniently converted into segmented images or bit data and then imported into the DMD-based bioprinter interface to fabricate desired geometries and shapes. The integration of multiple independent bioink injections further offered easy feeding of different materials with fast switching. Computational fluid dynamics (CFD) was used to assess the performance of the microfluidic system for multimaterial patterning. Various patterns were fabricated through this platform to validate its multimaterial bioprinting capability. We further evaluated the flexibility and biocompatibility of the platform to generate biomimetic heterogeneous tissue constructs by using bioinks loaded with multiple cell types, introduced from the microfluidic chips into the DMD bioprinter.

The DMD-based bioprinter uses UV light (up to 500 mW cm^{-2}) to polymerize a liquid prepolymer toward a solid structure (**Figure 1**). The DMD panel that is an array of reflective-coated micromirrors creates light patterns at high definition (i.e., 1050 × 920) and speed (10 kHz rate of switching). The digital state of each micromirror can be controlled as being either 0 (dark) or 1 (light-reflecting for photopolymerization) while the bioink is introduced to the focal plane of the projected image, leading to its crosslinking in a layer-by-layer fashion. We calibrated the image size by printing a single image featuring a grid pattern, and then measuring the grid by an optical microscope. The lateral resolution is theoretically limited by the physical size of DMD mirrors, which is 7.6 µm for the selected model; however, experimental printing resolution (i.e., smallest feature size) was determined at the order of 10 µm (Figure S1, Supporting Information). Simple patterns were used to show printing capabilities of our DMD-based bioprinter over a range of UV exposure parameters and photoinitiator concentrations. The photoinitiator concentration affected the time required to fully crosslink the hydrogel from seconds to minutes. The practical resolution of our bioprinter was further shown by printing parallel lines, in which it generated the line thickness down to ≈25 µm (Figure S1f, Supporting Information).

Different from existing DMD bioprinters, we developed a unique microfluidic device to turn our system into a multimaterial stereolithographic bioprinting platform. **Figure 2**a illustrates the design of the microfluidic device consisting of one poly(dimethylsiloxane) (PDMS) chamber featuring four inlets held between two poly(methyl methacrylate) (PMMA) sheets, which allowed for sequential injection of different bioinks (Figure 2b). The three branches in the middle region were introduced to widen the directionality of the washing flow and reduce flow forces imposed on the printed construct (as seen by experimental observations in Figure 2). Bioink flow filled the

Prof. A. Khademhosseini
California NanoSystems Institute (CNSI)
University of California-Los Angeles
Los Angeles, CA 90095, USA
Prof. A. Khademhosseini
Department of Bioindustrial Technologies
Konkuk University
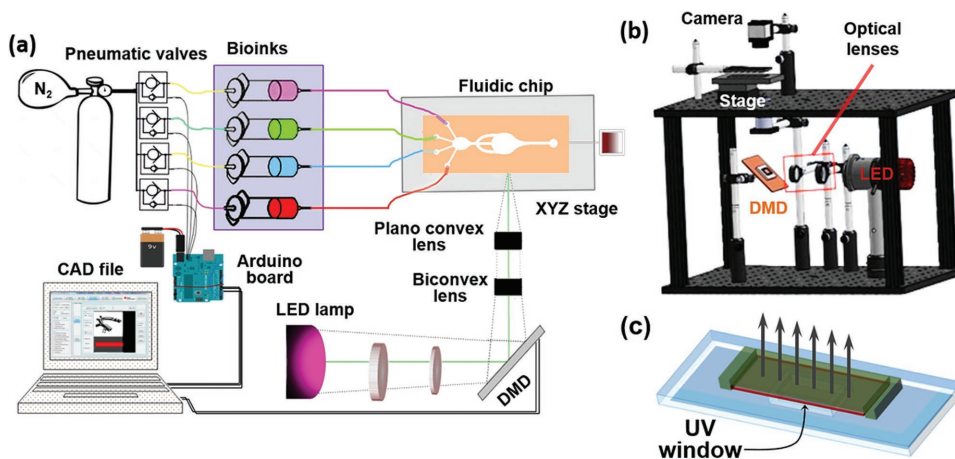Seoul 143-701, Republic of Korea

**ADVANCED
SCIENCE NEWS**

www.advancedsciencenews.com

**ADVANCED
MATERIALS**

www.advmat.de

Figure 1. a) Planar schematics showing the setup of the bioprinter, including a UV lamp (385 nm), optical lenses and objectives, a DMD chip, and a microfluidic device. b) Schematic showing the actual setup of the entire optical platform. c) Schematic showing an open-chamber microfluidic device used to create single-material printouts.

chip in a few seconds, before subjecting to UV crosslinking. Phosphate-buffered saline (PBS) then washed away the first bioink within the same time frame, and this was repeated for the second and following bioinks. In addition, we assessed

chip performance by tracking dye particles in dye-filled bioink flows within the microfluidic device and washing by the subsequent bioink (in a different color), or PBS. Figure 2c shows the simulation of our numerical model for flow patterns around
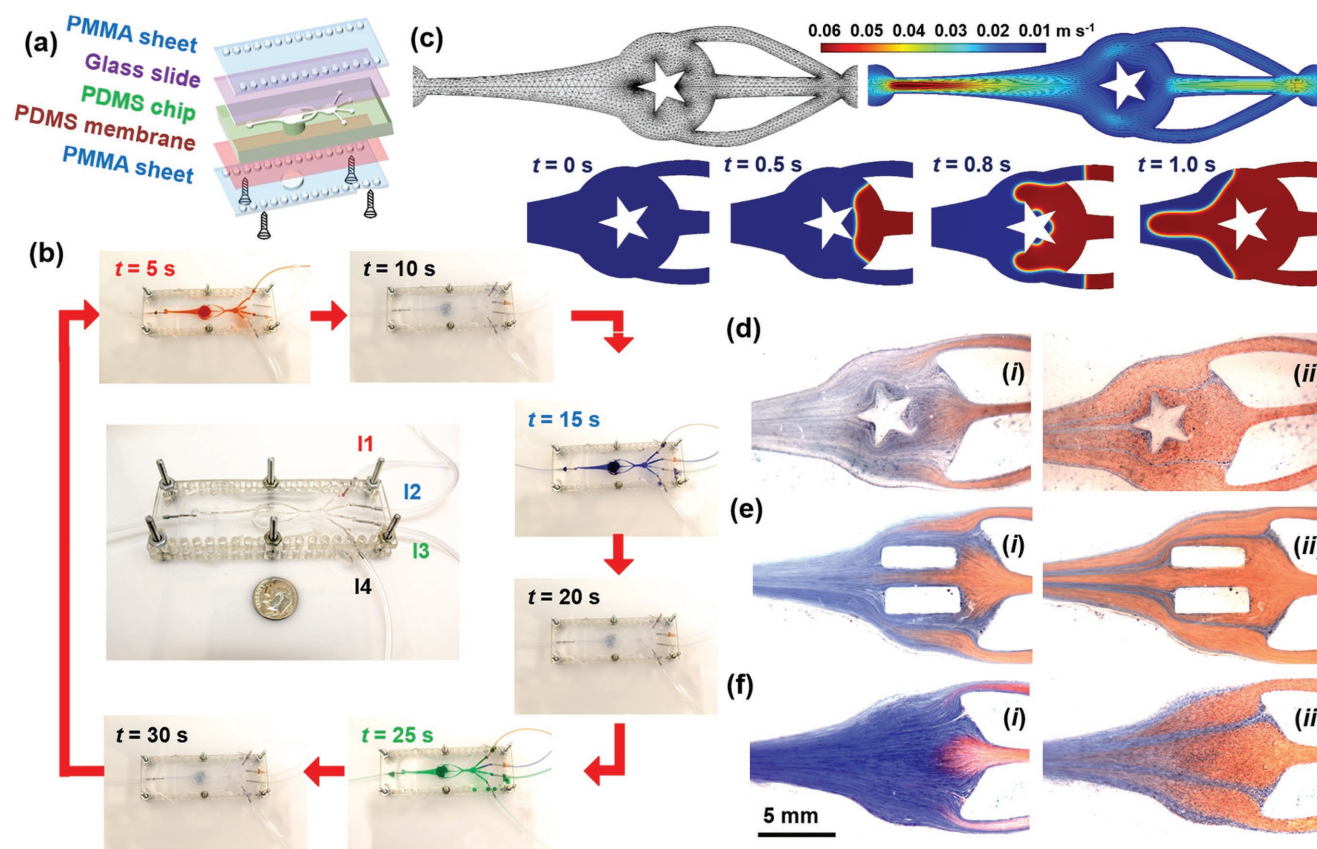

Figure 2. a) Schematic showing the assembly of the microfluidic chip having four inlets and one common outlet. b) The operation of the microfluidic device for consecutive injection of different bioinks and the washes in between the injections. c) The defined CFD model and the velocity profile (m s^{-1}) of PEGDA (with a density 1.06 kg m^{-3} and a viscosity 1×10^{-5} Pa s) in the closed chamber under sinusoidal fluid flow. d–f) The role of mixing and washing observed by flow streamlines in GelMA solution (15% w/v) mixed by food dye in the microfluidic chip for a star pattern, two rectangular patterns (made of PMMA molds), and no pattern, respectively.

**ADVANCED
SCIENCE NEWS**
www.advancedsciencenews.com

**ADVANCED
MATERIALS**
www.advmat.de

the star shape, indicating a close similarity (correlation coefficient >0.70) in the actual flow patterns observed around the star shape (Figure S2a, Supporting Information; left image vs right image). Figure 2d–f provides direct visualization on how the bioinks were washed when different shapes were printed inside the chamber. Despite the presence of branching and potential turbulence at edges, we were able to observe reasonable laminar flow in the printing region with a high-speed digital camera. As expected for microchannels, the viscous bioink was reaching to the printing region in a laminar regime (Reynolds number ≈ 10–100), which allowed smooth transition between sequential bioink injections. However, the shape of printed construct restricted the velocity and duration of bioink feeding. The bioink could be easily washed by the subsequent flow in the case of straight lines (Figure 2e), in the absence of any dead zone or low-speed streamlines in the flow (e.g., washing time ≈5 s at an inlet velocity of 1 cm s^{-1}). By contrast, flow patterns in the case of star shape showed low-speed streamlines inside the cavities that hampered the washing process, thus requiring bioink flow at higher speed or longer time (e.g., washing time ≈20 s at an inlet velocity of 1 cm s^{-1}). When there was no object present in the chamber the flow pattern was smooth (Figure 2f; e.g., washing time ≈2 s at an inlet velocity of 1 cm s^{-1}). Moreover, we investigated how the inlet pressure, regulated by the nitrogen tank, and the bioink viscosity could control maximum stress applied on the printed gel with a star shape (selected as a standard here). As summarized in Figure S2b,c of the Supporting Information, both stress and fluid velocity values were linearly correlated by inlet pressure or inlet velocity. This may allow the prevention of gel displacement by high shear stresses.

We further built an elastomeric membrane made of PDMS into our microfluidic chip, which undergoes vertical deformation during the bioprinting process to allow for the construction of 3D objects in conjunction with programmed injection of bioinks (**Figure 3**a,b). Starting from the first layer of crosslinking, the microfluidic chip moves up and this movement yields reduced deformation on the membrane, until its resting position (i.e., for a 5-mm-high printed construct). The resilience of the membrane was studied through numerical simulation and customized mechanical testing, as summarized in Figure 3c and Figure S3 (Supporting Information). The hyperelastic Neo-Hookean model[19] was used to simulate the deformation field and stress distribution of the PDMS membrane for the imposed boundary conditions (Figure S3, Supporting Information). The maximum deformation was under 50% strain when the chip was set at the initial position and it occurred at the contact region between the membrane and the rigid shell for the range of membrane thickness (from 200 to 500 μm). The central regions had uniform strains lower than 50%, and thus the deformation field is still within the elastic (i.e., reversible) range of PDMS.[20] Uniaxial tester was then employed to obtain load–displacement history of the membrane under vertical movements of the rigid shell (Figure S3, Supporting Information), where load–displacement curves showed hysteresis response depicting the role of friction forces on the membrane function. The membrane was programmed to load–unload when the chip was filled for printing each layer and subsequent washing, as depicted in Figure 3d; however, it was found that the presence of friction forces that yielded residual strain to a certain degree limited the number
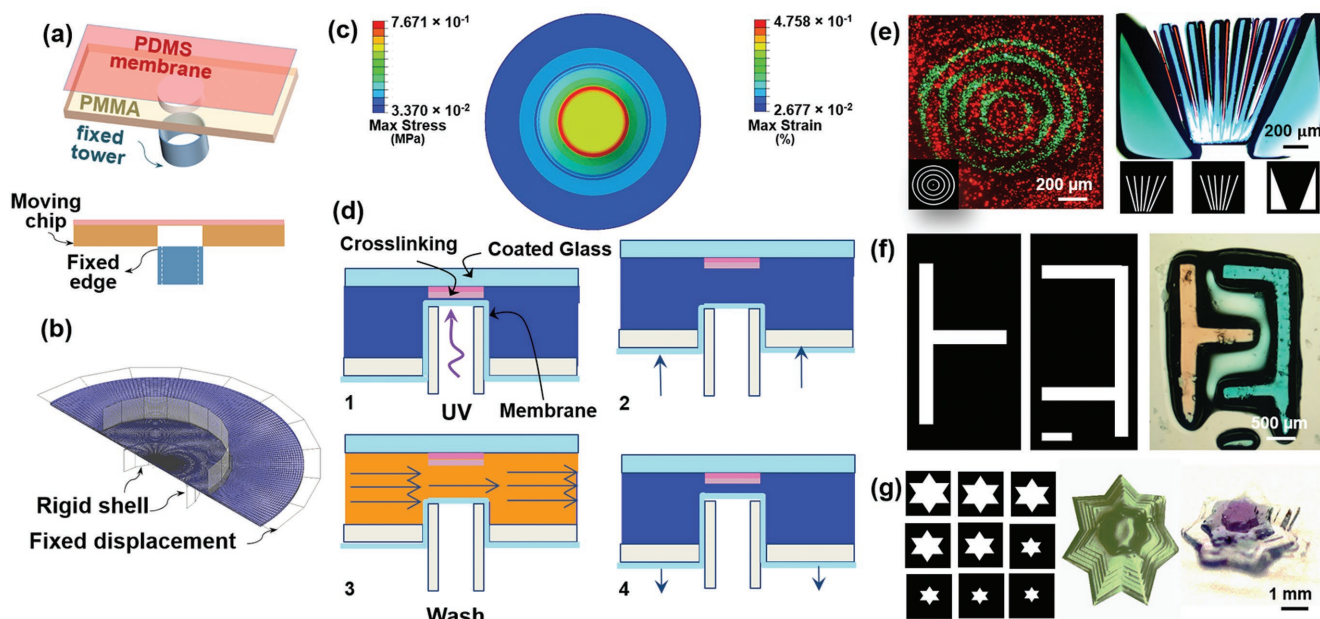

Figure 3. a) Schematic showing the microfluidic chip containing a moving part at the center of the bottom chamber. b) Computational domain of the finite element analysis built for an isotropic, incompressible, hyperelastic membrane supported on the rigid piston. c) Simulation result showing principle strain and stress values of the PDMS membrane at 4-mm displacement. d) Schematics showing the four-step bioprinting process inside the microfluidic chip for fabricating 3D objects. e–g) Examples of multicomponent bioprinted constructs: (e) a two-component GelMA-7% construct filled by fluorescent dyes (left) and a three-component pattern of colored PEGDA-50% (right); (f) a 3D fluidic mixer made by three different colors (white, orange, blue) printed from PEGDA-50%; and (g) a single-component (green) and a three-component (white, blue, purple, from bottom to top) star-shaped pyramid of PEGDA-50%.

of cycles for membrane deformation, requiring future optimization for printing a very high number of layers. In this work, we manually tightened the membrane after each construct with a relatively small thickness was printed and removed from the microfluidic chip. It should be noted that, the integration of such an elastomeric membrane is a unique feature in our multimaterial DMD platform as it functions to seal the microfluidic chamber during the exchange of the different bioinks while providing the ability of 3D bioprinting through layer-by-layer photocrosslinking. In comparison, in a conventional DMD or DLP setup the open-chamber design would not allow for efficient injection or washing of the bioinks, therefore prohibitive of multimaterial stereolithographic bioprinting.

We next demonstrated the capability of our bioprinter in generating two-dimensional (2D) and 3D constructs. Simple shapes with different materials were bioprinted using PEGDA (50% v/v) or GelMA (7% w/v) solution, containing 1–3 colored bioinks (Figure 3e–g). Constructs could also be fabricated in different shapes, such as eccentric circles, parallel, and oblique stripes, and pyramids of different base-shapes (see also Figures S1 and S4, Supporting Information). The planar printing resolution demonstrated the capacity of our bioprinting platform, while 3D bioprinting resolution was hampered by UV light scattering. It is noted that, while different bioinks

were sequentially injected into the microfluidic chip, there was no obvious sign of mixing, indicating successful washing of bioinks prior to crosslinking and the good performance of the elastomeric membrane in the microfluidic chip.

We further designed and bioprinted a set of sophisticated structures resembling biological tissues such as tumor angiogenesis, muscle strips, and musculoskeletal junctions (**Figure 4**ai,bi,ci). GelMA was used as a bioink due to its intrinsic cell-adhesion moieties that promote cell spreading and functionality.[21] Each organ-like structure had 2–4 different bioinks as each bioink was individually patterned in a rapid fashion, with smooth transitions among different bioinks. This transition that requires washing of bioink residuals in the bioprinting process can hamper cell viability as highlighted by a comparison of two different cases: single-component and two-component reticular constructs in Figure S5 of the Supporting Information.

The bioprinted structures possessed explicitly separated borders among different cell-laden bioinks, confirming the role of washing (Figure 4). The printing resolution was determined to be ≈20–30 µm, slightly reduced in comparison with noncellular patterns due to scattering of photons from cellular components.[22] Nevertheless, such a resolution is still compatible with our previous reports,[2] suggesting that the addition of the
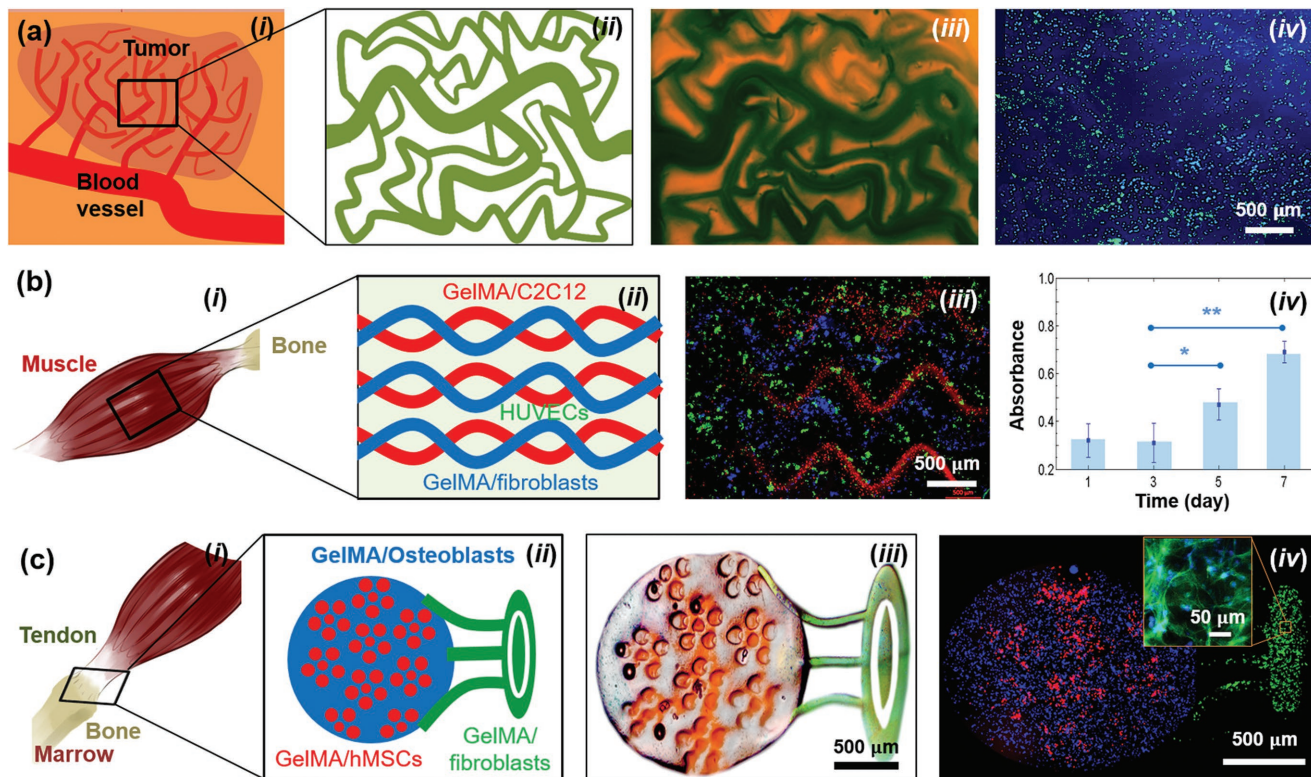

Figure 4. a) A tumor angiogenesis model: (i) schematic showing the tumor angiogenesis model; (ii) schematic of the mask for printing; (iii) bioprinted microvasculature in PEGDA; (iv) bioprinted MCF7 cell (blue)-laden microvascular bed of GelMA further seeded with HUVECs (green) in the channels. b) A skeletal muscle model: (i) schematic showing the skeletal muscle tissue; (ii) schematic of the mask for printing; (iii) bioprinted structure of GelMA containing patterned C2C12 cells (red) and fibroblasts (blue) after 48 h of culture; (iv) Presto blue measurements of cell proliferation in the bioprinted structures. c) A tendon-to-bone insertion model: (i) schematic of the tendon-to-bone insertion site; (ii) schematic of the mask for printing; (iii) bright-field optical image showing a bioprinted dye-laden GelMA structure; (iv) bioprinted structure of GelMA containing patterned osteoblasts (blue), MSCs (red), and fibroblasts (green); the inset shows a magnified image of the region hosting fibroblasts, where the cells were stained for f-actin (green) and nuclei (blue).

microfluidic chip in the current system to introduce multiple bioinks did not exert noticeable effects on the DMD stereolithographic bioprinting process.

One of the current challenges in cancer biology is to understand the complex, multicellular cancer microenvironment.[23] In vitro tumor cultures currently used in cancer research often result in different cell–matrix associations that in turn affect their functions;[24] to this end, bioprinting could become a promising strategy to engineering biomimetic cancer models due to its versatility in depositing cells and matrices in precisely defined manners.[25] Specifically, we printed a pattern mimicking angiogenesis in a matrix of GelMA laden with scattered breast cancer cells (MCF7), followed by introduction of human umbilical vascular endothelial cells (HUVECs) within the vascular channels, as shown in Figure 4a. Such a model, although primitive, could potentially allow studying the tumor progression and angiogenesis.

Models of the musculoskeletal systems were also fabricated using our multimaterial DMD-based bioprinter. Muscle bundle-like constructs were printed using two bioinks, loaded with NIH/3T3 fibroblasts and C2C12 skeletal muscle cells. The fluorescence image clearly revealed the capability of the system to print the spatially distributed cell-laden bioinks (Figure 4bii and iii), laying down the basis for future fabrication of functional muscular tissues containing hierarchical assembly of multiple cell types. The cell viability, determined immediately and at 1 and 7 d postbioprinting, indicated that all cell types maintained satisfactory proliferation and metabolic activity (Figure 4biv). In addition, we printed a construct mimicking the musculoskeletal interface integrating three different cell types, mesenchymal stem cells (MSCs), fibroblasts, and osteoblasts (Figure 4c). Again, the printed patterns were well-defined showing relatively strong similarity with the model (Figure 4ciii,iv vs ii).

The multimaterial capacity of our bioprinting platform was further assessed in vivo in a rat subcutaneous implantation model.[26] We designed a four-material construct made of PEGDA (35% v/v) as the framing structure and three GelMA strips with concentrations of 5%, 10%, and 15% w/v, respectively, as presented in **Figure 5**ai. Construct with vascular endothelial growth factor (VEGF) loaded in the GelMA strips was used as a positive control to stimulate angiogenesis (Figure 5aii,iii), where blank GelMA hydrogels served as the negative control. The implants were harvested at days 10 and 30 for histological examination (Figure 5aiv) and their gross appearances were first assessed. It has been previously reported that VEGF induces migration of multiple endothelial cell lines, such as capillary endothelium.[26,27] As depicted in Figure 5b, the presence of VEGF in the bioprinted multimaterial constructs did lead to the formation of more blood vessels
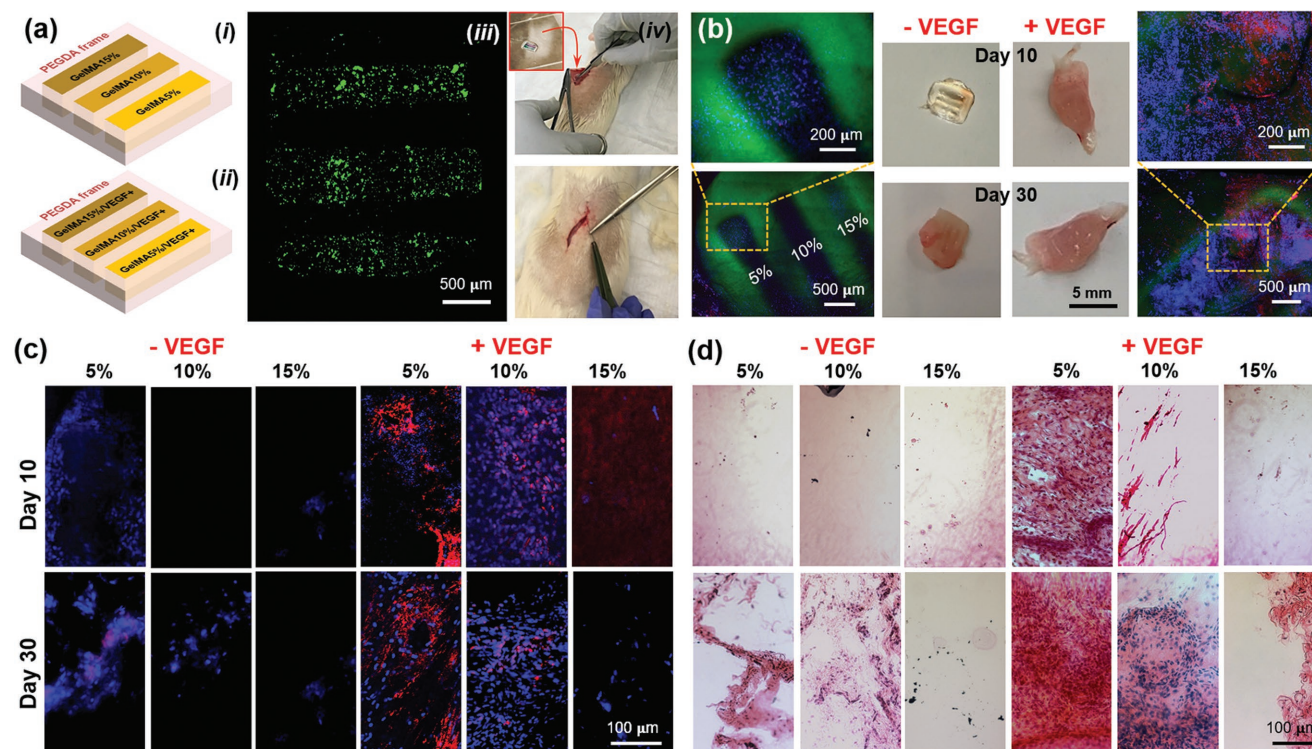

Figure 5. a) A concentration-gradient model generated by multimaterial DMD bioprinting: (i) schematic of the construct showing the PEGDA (35% v/v) frame and three GelMA strips of 5%, 10%, and 15% w/v concentrations with a uniform thickness of 1 mm; (ii) a bioprinted construct where the GelMA strips contained green fluorescent beads to mimic VEGF; (iii) the rat subcutaneous model used to assess the bioprinted constructs. b) Photographs showing the retrieved implants at day 10 and day 30, along with confocal images of the retrieved constructs at day 30 stained for nuclei (blue) and for CD31 (red), where the bright-field views were pseudocolored in green. c) Immunostaining of the retrieved implants for CD31 (red), for different GelMA concentrations (5%, 10%, and 15%), in the absence and presence of VEGF; the nuclei were counterstained with 4′,6-diamidino-2-phenylindole (DAPI) (blue). d) H&E staining of the retrieved implants for different GelMA concentrations, in the absence and presence of VEGF.

in the implants when compared to those without VEGF. The expressions of CD31 by the invaded cells were higher in the VEGF implants at day 10 compared to day 30 (Figure 5c). These results showed that encapsulated VEGF promoted the formation of the blood vessel network in the bioactive GelMA hydrogels, while the inert PEGDA served as the frame in the bioprinted multimaterial structure.

In addition, VEGF seemed to have induced more pronounced inward growth of the connective tissues along the peripheries of the implants (Figure 5b). Our hematoxylin and eosin (H&E)-staining results further demonstrated the inflammatory responses of the host to the implants and recruitment of inflammatory cells, particularly at the interfaces of connective tissues and implants (Figure 5d).[28] The differences in CD31 expression and connective-tissue formation were less distinctive between the 5% GelMA and the 10% GelMA compared to those in the 15% GelMA (Figure 5c,d). This may indicate that the higher concentration of GelMA (15%) prevented the invasion of cells into the implant possibly due to the denser polymer network and reduced rate of biodegradation. The in vivo study suggested our ability to fabricate heterogeneous constructs using the novel multimaterial stereolithographic bioprinting strategy to regulate desired biological functions such as angiogenesis.

In summary, we have demonstrated an innovative strategy by integrating a microfluidic device into the design of the DMD-based bioprinter to achieve, for the first time, automated, multimaterial stereolithographic bioprinting. In a typical process, our DMD-based bioprinting platform requires only a few seconds to perform washing (if switching is required); for example, we printed nonuniform constructs, composed of 2–3 bioinks, in less than 20 s, while an industrial DMD-based printer would probably consume an additional time of minutes simply devoted to manual bioink injections and switching.[16,29] Other manually operated laboratory-scale multimaterial DMD-based printers would take similar time to replace the bioinks.[2] Therefore, our bioprinter could achieve a speed faster than those of the existing stereolithography and/or DMD-based platforms. Such a speed may be further improved, through adopting a technique similar to that used in the continuous stop-flow lithography for photocrosslinking patterns within the same planes.[30] However, to achieve the bioprinting of 3D structures with distinct materials between the layers, our current bioprinting system still requires polymerization of the bioinks at static-flow conditions with the need of washing processes.

The advantage of our bioprinting platform in terms of fabrication speed would become more noticeable when fabrication time hampers cell viability in larger cell-laden constructs. The unique features of our bioprinter have significantly promoted the current level of control and printing speed among existing bioprinting techniques.[29,31] This concept is also expandable to as many bioinks as needed by simply increasing the number of inlet channels. In addition, the printing speed of our multimaterial DMD bioprinting system may be further improved by carefully coordinating projection light and local oxygen levels to achieve continuous photocrosslinking of the bioinks in a layerless manner.[32] The use of the proposed microfluidic chip, however, limited the physical size of the constructs that could be fabricated and the scale-up will demand alteration in the design of the chamber.

Experimental Section

DMD-Based Bioprinting Platform: Figure 1a shows the custom-built DMD-based bioprinting system used for the fabrication of multicomponent constructs. A UV LED (M385LP1-C1; Thorlabs, Newton, NJ, USA) mounted to a light collimator was used at a wavelength of 365 nm and a power of nearly 500 mW cm^{-2}. A Newport (Nashua, NH, USA) power meter was used to determine the light intensity. The digital models built with AutoCAD were converted to 2D bitmap slices and translated to spatially tilt a pattern of micromirrors on the DMD panel (DLP LightCrafter 6500; Texas Instruments Inc., Dallas, TX, USA). A stage controller was used to manage the three-axis stage movement, whereas the UV light source (Thorlabs) was directed via an optical path toward the DMD panel at a specific angle to facilitate light reflection through the projection optics to the stage. The thickness of the layers could be adjusted in 100-μm steps and the planar resolution of the system was found to be approximately 10 μm (with a 5 × 5-mm^2 illumination area). This resolution was achieved utilizing a compound lens with 2-cm working distance (Figure 1b). Since the DMD reflects an array of square pixels and the layers are built on top of each other, the tolerance of the printing is important in the resolution of constructs.[16] Exposure times ranged from 1 to 20 s depending on the aperture of light and hydrogel composition. The DMD panel, the stage, and the UV light source were controlled by a microcontroller (Arduino UNO; Arduino, Italy). Figure 2b shows the printing sequence controlled by the Arduino program. While the pattern is being printed there is no liquid flowing in the chamber (stage 1 in Figure 3d); once the pattern is printed, the motor brings the chip up (stage 2 in Figure 3d); if the material is to be changed, the valve of the next material is turned on, and the new material starts washing the one currently in the chamber (stage 3 in Figure 3d); an additional washing with buffer can be added if the material is hard to wash; finally, the motor brings the chip down to print the following layer. An open chamber shown in Figure 1c was also used to test single-material printing and characterize the optical setup.

Hydrogel Preparations: PEGDA ($M_n = 700$), 2,2,6,6-tetramethylpiperidine 1-oxyl (TEMPO), and gelatin from porcine skin type A were purchased from Sigma-Aldrich (St. Louis, MO, USA). TEMPO mitigates free radical migration distance leading to structural sharpness in high-aspect ratio constructs.[17] High-purity distilled water was generated by Millipore system with a resistivity reading of 18.2 MΩ upon collection. Lithium phenyl-2,4,6-trimethyl-benzoyl-phosphinate (LAP) was purchased from Allevi (Philadelphia, PA, USA). This photoinitiator is extensively used for cellular studies.[33] A 50% v/v PEGDA aqueous solution was prepared, and TEMPO (0.01% w/v) and LAP (1.0% w/v) were added to the solution. The mixture was heated to 80 °C for 1–3 h. The resulting PEGDA bioink was used to fabricate the structures presented in Figure S1 of the Supporting Information. Food dyes and fluorescence beads were used to assist visualizations when necessary. For 3D constructs and cell study GelMA-7% w/v solution containing LAP (0.3% w/v), as shown in Figure S4 of the Supporting Information, was used. GelMA was also fabricated following the well-established protocol.[34] In summary, gelatin was dissolved in PBS for 2 h at 60 °C under constant stirring to make a 10% w/v gelatin solution and then added 5% v/v methacrylic anhydride (Sigma-Aldrich), and subsequently stirred for 1 h at 60 °C and 500 rpm. Two volumes of preheated PBS were added and the solution was dialyzed for 1 week.

Multi-Inlet Microfluidic Chip: The microfluidic chip of the bioprinting platform (Figures 1a and 2a) was designed and fabricated. The chip model was designed using CorelDraw (Corel Corp, Ottawa, ON) software (see Supporting Information) and imported to a laser cutting machine (VLS 2.30 Desktop Laser, Universal Laser Systems Inc, Richmond, VA) for cutting PMMA sheets (1.6 mm in thickness; McMaster-Carr, Robbinsville, NJ, USA). The mold included four 1-mm wide inlets, connecting channels, one printing region of 10 mm in diameter, and one outlet. After merging the four inlets, the first semicircular region was 4 mm wide and it connected to a short 2-mm wide channel. A smooth connection was designed to the printing region with three curved branches so that the hydraulic resistance of each branch was

**ADVANCED
SCIENCE NEWS**

www.advancedsciencenews.com

**ADVANCED
MATERIALS**

www.advmat.de

approximately one-third the hydraulic resistance of one single channel. The four inlets were merged into a wider region (4 mm in width) with a total length of 5 mm. PDMS precursor (Sylgard 184; Dow Corning, Midland, MI), prepared by an elastomer/curing agent ratio of 10:1, was poured onto the PMMA mold, cured at 85 °C for 2 h, and peeled off. A circular region assigned for printing was created using a customized punch (outer diameter: 10 mm) in the center of the PDMS chamber. The design also included a thin PDMS membrane; spin-coating (at 1000 rpm) of a PDMS drop on a glass slide was used, followed by curing at 85 °C for 2 h, to achieve this membrane. The patterned PDMS replica was manually bonded to the membrane and then sandwiched between two PMMA sheets, as depicted in Figure 2a. To connect the inlets and outlet, stainless-steel adaptors (outer diameter: 0.5 mm) were used.

Supporting Information

Acknowledgements

Conflict of Interest

The authors declare no conflict of interest.

Keywords

[1] Y. Ozlem, L. Shih-Feng, S. Binil, *Biofabrication* **2009**, *1*, 045004.

[2] X. Ma, X. Qu, W. Zhu, Y.-S. Li, S. Yuan, H. Zhang, J. Liu, P. Wang, C. S. E. Lai, F. Zanella, G.-S. Feng, F. Sheikh, S. Chien, S. Chen, *Proc. Natl. Acad. Sci. USA* **2016**, *113*, 2206.

[3] B. R. Masters, *Annu. Rev. Biomed. Eng.* **2004**, *6*, 427.

[4] W. Sun, A. Darling, B. Starly, J. Nam, *Biotechnol. Appl. Biochem.* **2004**, *39*, 29.

[5] F. J. O'Brien, B. A. Harley, I. V. Yannas, L. Gibson, *Biomaterials* **2004**, *25*, 1077.

[6] L. Moroni, J. R. de Wijn, C. A. van Blitterswijk, *Biomaterials* **2006**, *27*, 974.

[7] F. P. Melchels, J. Feijen, D. W. Grijpma, *Biomaterials* **2010**, *31*, 6121.

[8] S. Michael, H. Sorg, C.-T. Peck, L. Koch, A. Deiwick, B. Chichkov, P. M. Vogt, K. Reimers, *PLoS One* **2013**, *8*, e57741.

[9] D. Dean, J. Wallace, A. Siblani, M. O. Wang, K. Kim, A. G. Mikos, J. P. Fisher, *Virtual Phys. Prototyping* **2012**, *7*, 13.

[10] G. Mitteramskogler, R. Gmeiner, R. Felzmann, S. Gruber, C. Hofstetter, J. Stampfl, J. Ebert, W. Wachter, J. Laubersheimer, *Addit. Manuf.* **2014**, *1*, 110.

[11] C. Sun, N. Fang, D. Wu, X. Zhang, *Sens. Actuators, A* **2005**, *121*, 113.

[12] J. Stampfl, H. Pettermann, R. Liska, *Biomimetics–Materials, Structures and Processes*, Springer, Berlin **2011**, p. 105.

[13] a) R. Raman, B. Bhaduri, M. Mir, A. Shkumatov, M. K. Lee, G. Popescu, H. Kong, R. Bashir, *Adv. Healthcare Mater.* **2015**, *5*, 610; b) Y. Pan, C. Zhou, Y. Chen, *J. Manuf. Sci. Eng.* **2012**, *134*, 051011.

[14] L.-H. Han, G. Mapili, S. Chen, K. Roy, *J. Manuf. Sci. Eng.* **2008**, *130*, 021005.

[15] J.-W. Choi, H.-C. Kim, R. Wicker, *J. Mater. Process. Technol.* **2011**, *211*, 318.

[16] V. Chan, J. H. Jeong, P. Bajaj, M. Collens, T. Saif, H. Kong, R. Bashir, *Lab Chip* **2012**, *12*, 88.

[17] J. Warner, P. Soman, W. Zhu, M. Tom, S. Chen, *ACS Biomater. Sci. Eng.* **2016**, *2*, 1763.

[18] A. P. Zhang, X. Qu, P. Soman, K. C. Hribar, J. W. Lee, S. Chen, S. He, *Adv. Mater.* **2012**, *24*, 4266.

[19] Y.-C. Fung, *Foundations of Solid Mechanics*, Prentice Hall, Englewood Cliffs, NJ **1965**.

[20] A. M. Nazari, A. K. Miri, D. M. Shinozaki, *Polym. Test.* **2016**, *52*, 85.

[21] D. Loessner, C. Meinert, E. Kaemmerer, L. C. Martine, K. Yue, P. A. Levett, T. J. Klein, F. P. W. Melchels, A. Khademhosseini, D. W. Hutmacher, *Nat. Protocols* **2016**, *11*, 727.

[22] L. Wang, S. L. Jacques, L. Zheng, *Comput. Methods Programs Biomed.* **1995**, *47*, 131.

[23] a) P. Carmeliet, R. K. Jain, *Nature* **2000**, *407*, 249; b) S. N. Bhatia, D. E. Ingber, *Nature* **2014**, *201*, 4.

[24] D. Nieto, R. Couceiro, M. Aymerich, R. Lopez-Lopez, M. Abal, M. T. Flores-Arias, *Colloids Surf., B* **2015**, *134*, 363.

[25] Y. S. Zhang, M. Duchamp, R. Oklu, L. W. Ellisen, R. Langer, A. Khademhosseini, *ACS Biomater. Sci. Eng.* **2016**, *2*, 1710.

[26] H. H. Oh, H. Lu, N. Kawazoe, G. Chen, *J. Biomater. Sci., Polym. Ed.* **2012**, *23*, 2185.

[27] J. J. Schumacher, R. P. Dings, J. Cosin, I. V. Subramanian, N. Auersperg, S. Ramakrishnan, *Cancer Res.* **2007**, *67*, 3683.

[28] E. M. Hetrick, H. L. Prichard, B. Klitzman, M. H. Schoenfisch, *Biomaterials* **2007**, *28*, 4571.

[29] R. B. Wicker, E. W. MacDonald, *Virtual Phys. Prototyping* **2012**, *7*, 181.

[30] a) D. Dendukuri, D. C. Pregibon, J. Collins, T. A. Hatton, P. S. Doyle, *Nat. Mater.* **2006**, *5*, 365; b) P. Panda, S. Ali, E. Lo, B. G. Chung, T. A. Hatton, A. Khademhosseini, P. S. Doyle, *Lab Chip* **2008**, *8*, 1056.

[31] W. Liu, Y. S. Zhang, M. A. Heinrich, F. De Ferrari, H. L. Jang, S. M. Bakht, M. M. Alvarez, J. Yang, Y.-C. Li, G. Trujillo-de Santiago, A. K. Miri, K. Zhu, P. Khoshakhlagh, G. Prakash, H. Cheng, X. Guan,

ADVANCED
SCIENCE NEWS

www.advancedsciencenews.com

ADVANCED
MATERIALS

www.advmat.de

Z. Zhong, J. Ju, G. H. Zhu, X. Jin, S. R. Shin, M. R. Dokmeci, A. Khademhosseini, *Adv. Mater.* **2016**, *29*, 1604630.

[32] J. R. Tumbleston, D. Shirvanyants, N. Ermoshkin, R. Janusziewicz, A. R. Johnson, D. Kelly, K. Chen, R. Pinschmidt, J. P. Rolland, A. Ermoshkin, E. T. Samulski, J. M. DeSimone, *Science* **2015**, *347*, 1349.

[33] Y. S. Zhang, F. Davoudi, P. Walch, A. Manbachi, X. Luo, V. Dell'Erba, A. K. Miri, H. Albadawi, A. Arneri, X. Li, X. Wang, M. R. Dokmeci, A. Khademhosseini, R. Oklu, *Lab Chip* **2016**, *16*, 4097.

[34] J. W. Nichol, S. Koshy, H. Bae, C. M. Hwang, S. Yamanlar, A. Khademhosseini, *Biomaterials* **2010**, *31*, 5536.